Dynamic data analysis for pediatric airways

Chun-Wei Liu

November 8, 2014

Abstract

The analysis of pediatric airway geometry using computed tomography (CT) images has provided rich diagnostic cues for doctors. Recently, dynamic CT data has started to provide a better characterization of pediatric airways throughout the breathing cycle, for example to assess tracheomalacia. However, how to preprocess the increasing amount of dynamic data and how to analysis these data are still open questions. In this work, I performed dynamic data analysis using computer vision and machine learning approaches on synthetic and real airway data. In the future, I aim at building a 4D atlas for pediatric airways and to extend the approaches to other dynamic data modalities.

1 Introduction

The analysis of pediatric airway geometry using 3D computed tomography (CT) images has provided rich cues for doctors to diagnose respiratory issue for patients. Both radiologists and physicians have been working on the field for a while. In image analysis side, radiologists started to propose algorithm for measuring airway lumenal area using multidetector row CT [1] over the past decade. In the other respects, physicians adopted benefits from imaging analysis for their clinical studies, for example, how well their patients with issues caused by airway were recovered after surgeries [2]. The progress made in image analysis these days was making the communication of both parties much easier by providing more informative statics from images. For instance, given a CT image from a subject with some manually annotative landmarks, machine is able to learn from CT images of normal control data to build a subject-specific control atlas (a mean statics from the population of the subject.) Then machine can provide statics for where the positions have smaller cross-sectional area to doctors which makes diagnosing tracheal stenosis more actuary [3].

What can we learn from a four-dimensional CT (4D) image, an image set contains up to 16 3D CT images with respiratory motion induced image changes across the set that are not available on a single-component 3D CT image? If an edge of 3D CT images, comparing with spirometry, is on answering *where* a respiratory issue might be caused in the airway. Then, 4D CT images provide even more information about *when* the respiratory issue might be caused in a respiratory cycle.

Four-dimensional CT imaging was developed to provide an estimate of tumor motion for radiotherapy treatment planning [4]. After then, a method for dynamic ventilation imaging of the full respiratory cycle from 4D CT images was developed [5]. Recently, 4D CT imaging has started to provided a better characterization of pediatric airways throughout the breathing cycle, for example to assess tracheomalacia, which is a disease of temporally collapse of partial airway.

However, how to preprocess the increasing amount of dynamic data and how to analysis these data for pediatric airways are still open questions. While standard techniques for analysis 3D CT images could be applied on analysis 4D CT images in a frame-by-frame fashion, two major challenges can be addressed as follow. First, manual annotation labors or preprocessing costs of each subject has increased a factor proportional to the number of CT scans in a breath cycle. Second, no information sharing between time steps makes temporal inconsistence for the analysis. In this work, I am going design an automatically 4D data processing framework to address the above issues by performing dynamic data analysis using computer vision and machine learning approaches.

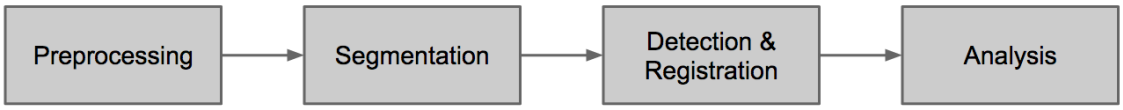

Figure 1: Illustration of the proposed 4D CT image processing framework. From CT image preprocessing, image segmentation, landmark detection and functional data registration, to final analysis.

In Section 2, I will introduce the framework applying on pediatric airway analysis. Experiments on real airway data would be compiled in on Section 3. In Section 4, I will discuss about the future works, including building a 4D atlas for pediatric airways and extending the approaches to other dynamic data modalities.

2 Methods

In terms of analysis subjects with huge varieties, including age, weight, and length of airway, data registration is an important issue. To compare different subjects in one metrics, registration between different subjects for compensating the deformation is needed for atlas building. Along with inter-subject registration, intra-subject registration to different scans in a period of time in critical. Registration within a subject in a short period of time would be much tractable for registration among different subjects. Several registration techniques have been developed in different perspectives. First, registration on image, which uses image intensity as a major feature, has being developed in medical image analysis for past decade. Most of these methods have to do with defining an energy function with data term (dissimilarity between source image and target image) and regularization term (atypicality of mapping from source image to target image), and then develop optimization method to find a best mapping which minimizes such energy. Hill et al. and Sotiras et al. wrote very educated review articles on general registration methods on image intensity [6, 7]. For particular application for registration on one subject among a short time period, Guerrero et al. developed a deformable algorithm for dynamic ventilation imaging from 4D CT [5]. Besides, registration on shape, which uses geometric cues as major features, has succeeded in many applications in computer vision and computer graphics fields [8, 9]. With the same fashion of energy minimization framework as image registration, these methods rely on shape features, e.g. curvature or level of bending, to define the data term. However, applying those techniques above for aligning pediatric airway 3D CT scans among different subjects was still a hard problem. No even mention we have variances within each subject due to 4D CT scans. Hong et al. proposed a simplified airway model which is much easier to register for further analysis [3]. I started this project by extending Hong et al.'s simplified airway model to a 4D CT processing framework. Figure 1 illustrated the automatic 4D CT processing framework.

2.1 Image preprocessing and segmentation

For better adaptive to currently medical image processing libraries, the framework start with transform data from DICOM images to NRRD images. Then a padding and filtering operator for making the image boundary has the same intensity as air is applied on NRRD images. With scripts automatically applying preprocessing programs reduced cost of manually operating medical image softwares, such as Slicer or ParaView.

The algorithm segmented the airway from 3D CT image using Otsu's method and two manually chosen seeds that bracket the upper airway. Otsu's method finding a threshold to separate data into two clusters, so as to try to make each cluster as tight as possible. This is achieved by maximizing the inter-subject variances and minimizing intra-subject variances in terms of voxel intensity. In our case for segmenting airway, the two clusters were air and non-air regions. To remove the air regions that were not in the airway, morphological operator erosion first be applied to remove the actual airway. This computed a map of outside air regions. We can apply the map as a filter to remove the air outside the airway to get a clean airway in the subject. Then, two seeds further help to extract trachea and exclude bronchus in the airway.

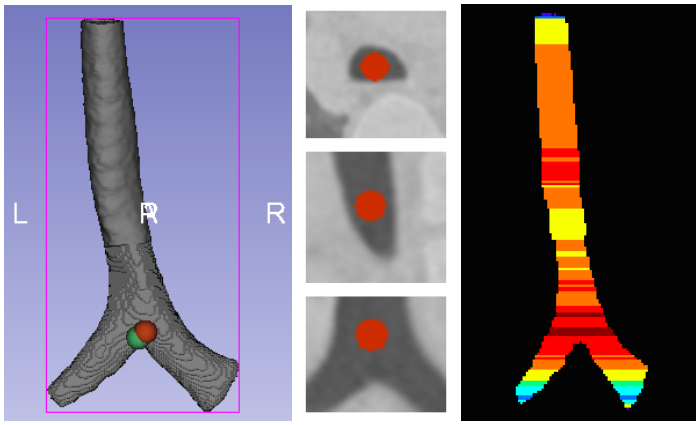

Figure 2: Visualization of the framework of landmark detection. **Left.** First, an airway geometry is segmented by Otsu-thresholding. Green marker is the ground truth annotation and red marker is the predicted location of TC. **Middle.** Second, CHOG features are computed in the center of trachea in each depth. From top to down: Sagittal, coronal, and axial. **Right.** Final, applying the trained classifier on these different hypotheses to get likelihoods of the landmark. Dark red indicates the highest likelihood of TC. In this case, the predicted TC has only 1.97 mm (the total length is 159 mm) away from the ground truth annotation. This error is only 1.2% of the entire airway.

With this segmentation, the upper airway can be approximated by statical models, including boundary point distribution models, deformation of atlas models, implicit models, or skeletal models [10]. Focus on measuring the size of airway, we used a centerline with cross sections to represent the airway. The centerline is inferred based on the heat distribution along the airway flow that is solved by a Laplace equation. Cross sections are cut from segmented airway geometry using planes that are orthogonal to the centerline. The area of the cross sections would be the 1D functional data representation of an airway.

2.2 Landmark detection

We can register functional data alone with some common landmarks across subjects. In general, landmark annotation was performed manually. For reducing the manually annotation cost, based on Dalal and Triggs's object detection framework [11], I propose a landmark detection framework using concatenating Histogram of Gaussian (CHOG) features and geometric prior. Figure 2 illustrated a detection of trachea carina (TC).

HOG is well designed normalized local histograms of image gradient orientation in a dense sample grid. The original purpose of this feature was for human detection. Given the popularity of HOG based object detectors, researchers even tried to answer why it works (or did not work) by visualizing the feature spaces [12]. Nevertheless, HOG captures edge or gradient structure that is very characteristic of local shape in our cases, and it can be efficiently computed. In practice the HOG is implemented by dividing an image window into small spatial cells, for each cell accumulating a histogram of gradient directions with different bins over pixels of the cell. The concatenated histogram over cells would be the final representation of an image window.

For applying HOG on 3D images, instead of computing histogram over arbitrary 3D orientations, I attempted to computed 2D HOG in axial, coronal, and sagittal plane, which are the three perspectives for user annotations. This reduced the computational complexity and made learning feasible given limit amount of ground truth images.

The first step of the landmark detection framework then is to train a binary classifier using CHOG. For doing high dimensional data and low sample size statical analysis, Distance Weighted Discrimination can be applied to improve the training [13]. Yet, for simplistic and speed, linear Support Vector Machine (SVM) is used as a baseline throughout study.

In prediction stage, the trained classifier can be applied as a filter on hypotheses with different locations and sizes. Higher score generally implies a higher likelihood of a hypothesis.

After landmarks are located, I registered the functional data to the unified domain [14]. In Hong et al.'s original paper, each subject had five visible landmarks from nasal spine, choana, epiglottis tip, true vocal cord (TVC), and TC. In our dynamic data, most of subjects only have TVC and TC. Even thought, in some cases, TC is the only available landmark which makes alignment impossible using current approach. Then, a heuristic assumption would be embedded to these special cases. The assumption is the subject has the same length of trachea from TVC to TC with the most relevant subject (in terms of age) in our control data. Therefore, we can compute the portion of the existed trachea by measuring the ratio of the length of current trachea in physical space and the length of the most relevant subject from TVC to TC.

2.3 Statical atlas analysis

Given special aligned functional data, I would like to capture population changes with respect to some factors, say age. A kernel regression approach can achieve the objective by assigning weights to data-object with respect to age. For example, I used Gaussian weight function $w_i(a_i; \sigma, \bar{a}) = c \exp{(a_i - \bar{a})/2\sigma^2}$, where a_i is the age for the observation i, σ is a predefined standard deviation and c is the normalization constant for fitting data to a specific age. To further analyze the weighted data, I applied weighted functional boxplots to build statical atlas for each dynamic subject [15].

Functional boxplots was originally proposed by Sun and Genton [16] which requires a definition of band depth for functional data. Band depth is a rank of functional data for ordering it from the center outward. Basically, the idea is the more subsets to which a data is belonged, the more centrality that data might have. Given a set of functional data $Y = \{y_i | i = 1, ..., n\}$, a combinatorial function C which enumerates all two pair combinations in a set, and a band function $B(y_1, y_2) = \{(t, x(t)) : t \in \mathrm{T}, \min(y_1(t), y_2(t)) \leq x(t) \leq \max(y_1(t), y_2(t))\}$, the band depth D of a functional data y with respect to a set Y can be defined as

$$D(y; Y) = \sum_{y_i, y_j \in C(Y)} I[y \subset B(y_i, y_j)], \tag{1}$$

where I is an indicator function. A general version of band depth is weighted modified band depth

$$D'(y; Y) = \sum_{y_i, y_j \in C(Y)} w_i w_j \lambda[B(y_i, y_j)] \tag{2}$$

where λ is the Lebesgue measure, and ws are the weights of kernel regression. The measurement of membership of a functional data is relax in (2), and it is based on a weighted populations which fits our objective.

When a rank of functional data is available, we can compute interesting statics such as median, interquartile range, and outliers of the population. I applied (2) to compute population atlas and plot subject dynamics upon the population atlas using (1).

3 Experiments

I applied the proposed framework on real world dynamic data. This section would reveal more implementation details and parameter settings, and also provide results and observations from experiments.

3.1 Landmark detection results

First I conducted a prior experiment before further developing landmark detection techniques by answering the question: How would landmark dynamics affect final airway analysis?

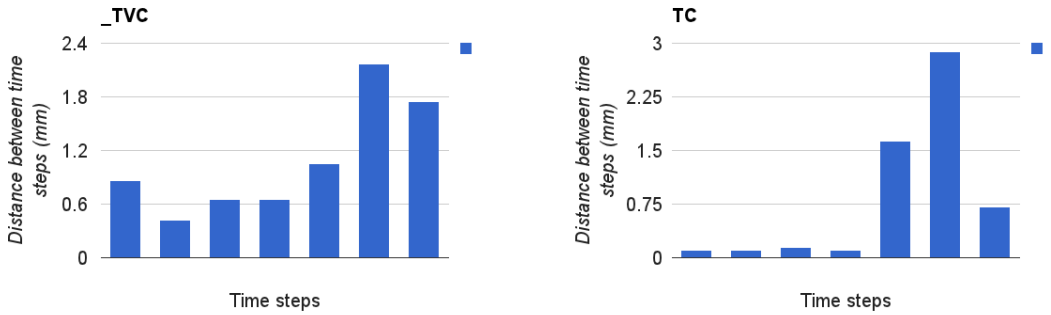

Figure 3: Visualization of the landmark dynamics of a 59 days subject.

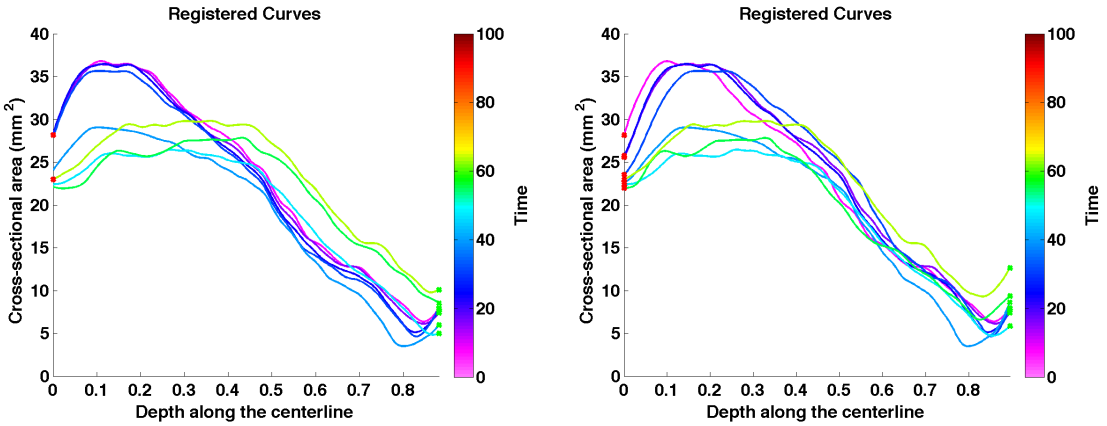

Figure 4: Cross-sectional area of a 59 days subject with different registration landmarks. **Left.** The result with same landmarks. **Right.** The result with updated landmarks. Note that in depth around 0.8, a lower cross-sectional measurement was disappear in the left but remained in the right.

I studied this on the first dynamic data I got from a doctor. This 59 days subject only had a dummy TVC [1] and TC for registration. I manually annotated the these two landmarks in each frame and computed the Euclidean difference between landmarks with respect to time.

Figure 3 showed the landmark dynamics between each frame in millimeter. In this figure, TC had a significant changes after time step 4. The landmark dynamics revealed that airway of the subject was changing a lot in a period of time. This observation matched our measurement of cross-sectional areas.

Figure 4 showed the results of airway measurement of the 59 days subject. The different between two is whether considering the landmark dynamics. One neglected landmark dynamics and the other used updated landmarks in each time steps. We can see that Figure 4 (right) captured a cross-sectional area drop around depth 0.8. Figure 4 (left), however, lost this feature (aware difference between the green curves on the left and on the right.) Because an area drop is a critical feature for airway analysis, I considered updating landmarks in each time frame is an important issue and further developed the framework described in Section 2.2.

Training. The training set had 95 3D CT images with manually annotated landmarks from nasal spine, choana, epiglottis tip, TVC, and TC. I trained a linear SVM classifier for TC using CHOG features. Each subject provided a positive example which would be HOG features extracting from three orthogonal bounding boxes passed through the landmark TC. The scale of the bounding boxes was determined by twice of the

[1] TVC was not visible due to the doctor's choice of scan area. I then chose the top of the airway as a dummy landmark TVC

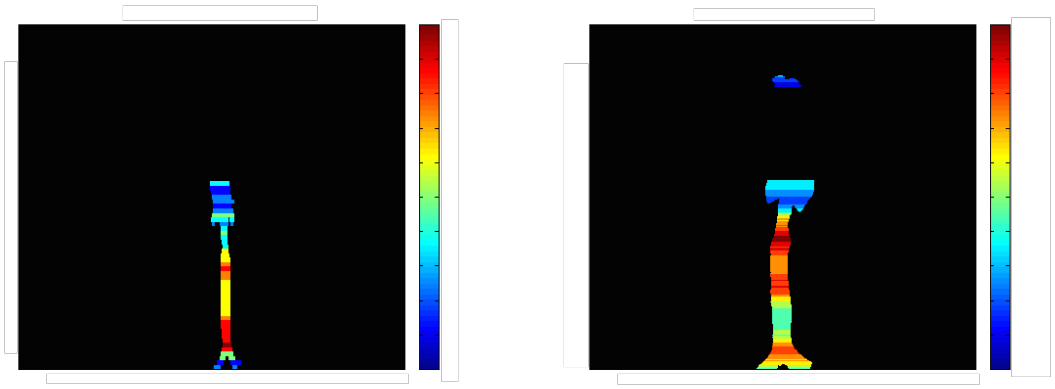

Figure 5: Illustration of the likelihood of landmark TC. **Left.** In most cases the detector located TC in a correct position. **Right.** Even fail cases still nominated the correct position as their second/third choice.

Table 1: Errors of landmark prediction methods of a 134 month subject (Fleck-005).

	mean (mm)	std. (mm)	mean (px)	std. (px)
None	4.7575	2.5314	18.6614	10.2052
CHOG	2.8812	1.6134	9.3357	6.6279

minimum rectangle covered the airway in the axial plane. The negative examples were drawn in random scale and location that not intersected with the positive bounding boxes.

Detection. In our case, I utilized a prior of geometry to eliminate possible hypotheses. In each depth I only drew one hypothesis from the center of the airway using the scale with the same heuristic in training. The trained SVM classifier predicted a score of the landmark likelihood given different depth. Figure 5 illustrated the likelihood prediction on training data. We can see there are some outliers in prediction on the training data. Due to these outliers, the mean prediction error was 24.7436 (mm) and the standard divination was 29.4251 (mm).

Now let us try to apply the detector on dynamic data and see if it can handle landmark dynamics against the system dynamics. I applied the detector on a 134 month subject (Fleck-005). Table 1 summarized the errors of landmark prediction on TC for which neglecting landmark dynamics, and my landmark detector using CHOG[2]. My automatically landmark detector reduced the errors of the mean and standard deviation. However, the problem of outliers reminded in one time frame. The current landmark detection framework did a decent job yet there are some spaces of improvement.

3.2 Dynamic airway analysis

I performed dynamic airway analysis using functional boxplots on real world data given by a physician. The normal control atlas was built from 68 health subjects in control group used the method in [3]. Figure 6 showed the results. Here I compared these results with the comments from the doctor of two cases.

Fleck-007, 114 months. It seemed to have a narrow airway on the CT scan in the first glance. However, comparing with the normal control atlas, this subject definitely had edge in term of size of airway. Also, the doctor gave the comment "No significant change in the trachea or bronchi during cough maneuver. No evidence of tracheobronchomalacia.", which agreed with the analysis.

[2]One outlier is removed. Count the outlier than the mean would be 3.9280 mm (12.7448 px) and the std. would be 4.4680 mm (15.0649 px).

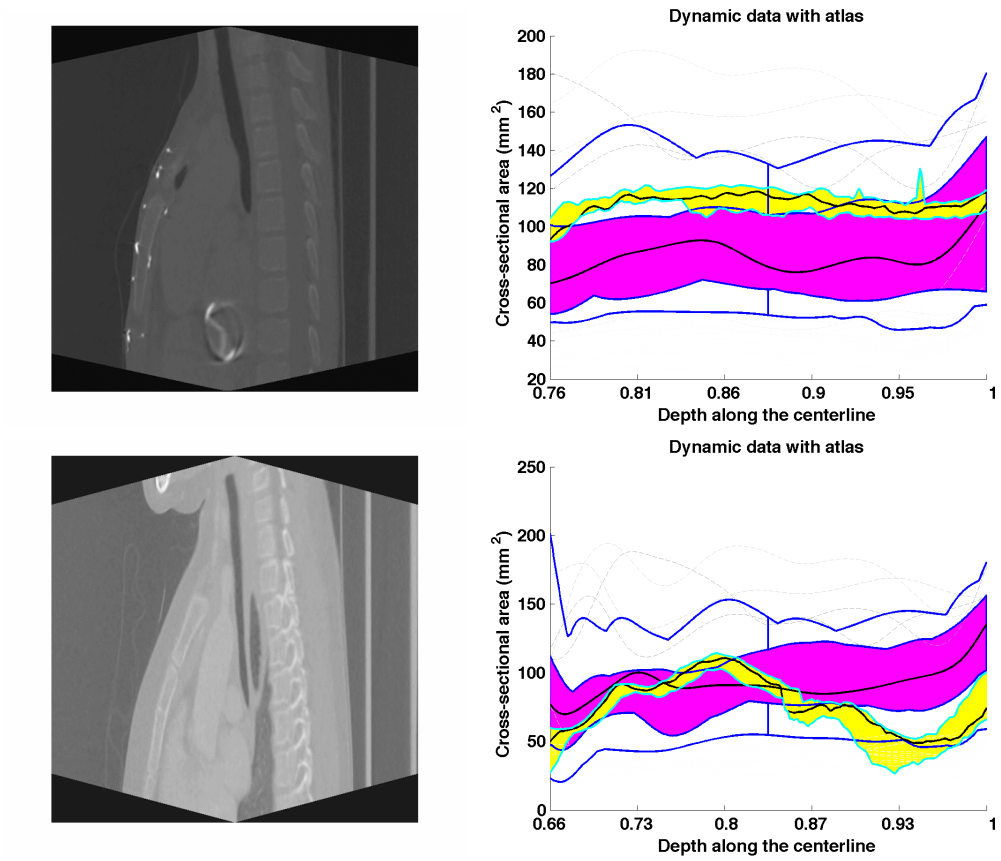

Figure 6: Dynamic airway atlas for subject Fleck-007 and Fleck-008. **Left.** A slice of dynamic data. **Right.** The purple area is the interquartile range of normal control atlas. The blue curves are the boundary of the normal control atlas. The yellow area is the entire estimation range of the dynamic subject in different time steps. The depth is in a unified scale, where 0.66 is TVC and 1 is TC.

Fleck-008, 129.6 months. The airway seemed normal in one slide. Yet it was considered narrowed comparing with the normal control atlas, and it had large dynamics especially from the depth 0.87 to 1. Quote the doctor's comment "Dynamic, 2.5 cm long narrowing of the mid to distal thoracic trachea caused by the adjacent left-sided aortic arch. The luminal diameter of the trachea changes from 11 mm during diastole to 5 mm in systole", the subject did have problem on the mid to distal thoracic trachea, which agreed with the observation.

4 Discussion

This work proposed an automatic framework for processing a 4D CT image of pediatric airway and providing informative visualization for further analysis. The current approach of data registration using detected landmarks has two issues. First, the detection has outliers. The outliers could be eliminated by examination the distance of each detected result between the detection mean. Yet more powerful features might need to be developed. Second, finding correspondents between a subject without enough landmarks to its statical atlas is handled by heuristics. To fully solving this problem, reducing the rely on landmarks is necessary. Since the within subject deformations were not dramatic, as Guerrero et al.'s suggestion in [5], a deformable image based registration within a subject would be a proper next step. While the results has showed dynamic

ranges and a comparison between dynamic data to normal control atlas, a more straight forward metrics which quantifies atypicality of subjects would be very appreciated. A reasonable next approach would be designed a metrics to evaluate the dynamics of airway. A long term goal of this project is to develop a theory of 4D CT atlas building of pediatric airways and aim for going beyond to other parts of human body.

References

[1] Nakano, Y., Whittall, K.P., Kalloger, S.E., Coxson, H.O., Flint, J., Pare, P.D., English, J.C.: Development and validation of human airway analysis algorithm using multidetector row ct. In: Medical Imaging 2002, International Society for Optics and Photonics (2002) 460–469

[2] Abramson, Z., Susarla, S.M., Lawler, M., Bouchard, C., Troulis, M., Kaban, L.B.: Three-dimensional computed tomographic airway analysis of patients with obstructive sleep apnea treated by maxillomandibular advancement. Journal of Oral and Maxillofacial Surgery **69**(3) (2011) 677–686

[3] Hong, Y., Davis, B., Marron, J., Kwitt, R., Singh, N., Kimbell, J.S., Pitkin, E., Superfine, R., Davis, S.D., Zdanski, C.J., et al.: Statistical atlas construction via weighted functional boxplots. Medical image analysis **18**(4) (2014) 684–698

[4] Ford, E., Mageras, G., Yorke, E., Ling, C.: Respiration-correlated spiral ct: a method of measuring respiratory-induced anatomic motion for radiation treatment planning. Medical physics **30**(1) (2003)

[5] Guerrero, T., Sanders, K., Castillo, E., Zhang, Y., Bidaut, L., Pan, T., Komaki, R.: Dynamic ventilation imaging from four-dimensional computed tomography. Physics in medicine and biology **51**(4) (2006)

[6] Hill, D.L., Batchelor, P.G., Holden, M., Hawkes, D.J.: Medical image registration. Physics in medicine and biology **46**(3) (2001) R1

[7] Sotiras, A., Davatzikos, C., Paragios, N.: Deformable medical image registration: A survey. Medical Imaging, IEEE Transactions on **32**(7) (2013) 1153–1190

[8] Belongie, S., Malik, J., Puzicha, J.: Shape matching and object recognition using shape contexts. Pattern Analysis and Machine Intelligence, IEEE Transactions on **24**(4) (2002) 509–522

[9] Li, H., Luo, L., Vlasic, D., Peers, P., Popović, J., Pauly, M., Rusinkiewicz, S.: Temporally coherent completion of dynamic shapes. ACM Transactions on Graphics (TOG) **31**(1) (2012) 2

[10] Pizer, S.M., Jung, S., Goswami, D., Vicory, J., Zhao, X., Chaudhuri, R., Damon, J.N., Huckemann, S., Marron, J.: Nested sphere statistics of skeletal models. In: Innovations for Shape Analysis. Springer (2013) 93–115

[11] Dalal, N., Triggs, B.: Histograms of oriented gradients for human detection. In: Computer Vision and Pattern Recognition, 2005. CVPR 2005. IEEE Computer Society Conference on. Volume 1., IEEE (2005) 886–893

[12] Vondrick, C., Khosla, A., Malisiewicz, T., Torralba, A.: Hoggles: Visualizing object detection features. In: Computer Vision (ICCV), 2013 IEEE International Conference on, IEEE (2013) 1–8

[13] Marron, J., Todd, M.J., Ahn, J.: Distance-weighted discrimination. Journal of the American Statistical Association **102**(480) (2007) 1267–1271

[14] Ramsay, J.O.: Functional data analysis. Wiley Online Library (2006)

[15] Hong, Y., Davis, B., Marron, J., Kwitt, R., Niethammer, M.: Weighted functional boxplot with application to statistical atlas construction. In: MICCAI 2013. Springer (2013) 584–591

[16] Sun, Y., Genton, M.G.: Functional boxplots. Journal of Computational and Graphical Statistics **20**(2) (2011)